MODELING OF CONJUGATE HEAT TRANSFER USING GALERKIN APPROACH

Andrej Horvat*, Ivan Catton°

* Reactor Engineering Division, Institute "Jožef Stefan", Ljubljana, Slovenia,

° Morrin-Martinelli-Gier Memorial Heat Transfer Laboratory,
Department of Mechanical and Aerospace Engineering, University of California, Los Angeles

ABSTRACT

An algorithm for simulation of conjugate heat transfer in an electronic chip heat sink is described. Applying Volume Averaging Theory (VAT) to a system of transport equations, a heat exchanger structure is modeled as a homogeneous porous media. The interaction between the fluid and the structure, the VAT equation closure requirement, is accomplished with drag and heat transfer coefficients taken from the available literature and inserted into a computer code. The system of partial differential equations is solved using the Galerkin method to decompose the temperature field into a series of eigenfunctions.

An example calculation is performed for an aluminum heat sink exposed to force convection airflow. The geometry of the simulation domain and boundary conditions follow the geometry of the experimental test section used in the Morrin-Martinelli-Gier Memorial Heat Transfer Laboratory at University of California, Los Angeles. A comparison of the whole-section drag coefficient C_d and Nusselt number Nu as functions of Reynolds number Re_h shows good agreement with finite volume method results as well as with experimental data. The calculated temperature fields reveal the local heat flow distribution and enable optimization of the surface geometry.

INTRODUCTION

Heat exchangers can be found in a number of different industrial sectors where need to transport heat between media exist. Consequently, wide spread use of heat exchangers has caused development to take place in a piecemeal fashion in a number of rather unrelated areas. The technology of heat exchangers, familiar in one sector, has progressed slowly across the boundaries of the different sectors [1].

To overcome historic differences, a unified description of heat and fluid flow in heat exchange devices needs to be found. For this purpose, we chose Volume Averaging Technique (VAT), first presented by Whitaker [2] and further developed by Travkin and Catton [3-4], as one of the suitable options. By applying VAT to a system of equations, transport processes in a heat exchanger can be modeled as a homogeneous porous media flow. The interactions between fluid flow and heat sink structure, the VAT equations closure requirements, need additional modeling or experimental values.

In the present paper VAT was used to model heat transfer processes in an electronic chip heat sink. The geometry and boundary conditions closely followed the heat sink configuration experimentally studied in the Morrin-Martinelli-Gier Memorial Heat Transfer Laboratory at University of California, Los Angeles.

The system of transport equations resulting from application of VAT were solved semi-analytically using the Galerkin approach for Reynolds number ranging from Re_h = 164 to Re_h = 1898. In our case the definition of Reynolds number was based on a hydraulic diameter of a hypothetical porous media channel (eq. 24).

To demonstrate the usefulness and accuracy of the method, the results were compared with experimental [5] as well as with other numerical results [6]. Despite simplifications, which were needed to solve the problem semi-analytically, the comparison shows good agreement. The calculated temperature fields reveal the local heat flow distribution and enable the optimization of the surface geometry.

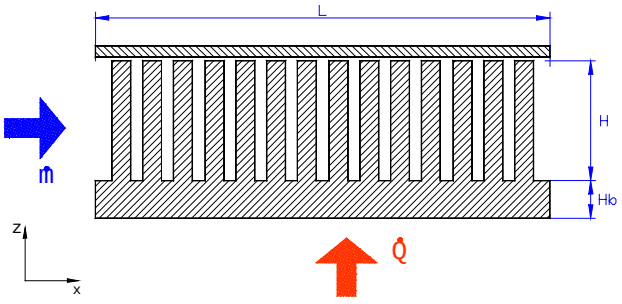

Figure 1: Experimental test section.

MODEL APPROACH

The airflow through an Al chip cooler structure can be described with basic mass, momentum and heat transport equations [6]. In order to develop a unified approach for heat exchanger calculations, the transport equations were averaged over a periodic control volume (see [4] for details). This Volume Averaging Technique (VAT) leads to a closure problem, where interface exchange of momentum and heat between fluid and solid have to be described with additional empirical relations e.g. a local drag coefficient C_d and a local heat transfer coefficient h.

To further simplify the simulated system, fluid flow was taken as unidirectional with a constant pressure drop. As a consequence, the velocity changes only vertically in *z*-direction. This means that the streamwise pressure gradient across the entire simulation domain is balanced with hydrodynamic resistance of the structure and with shear stress. Thus the momentum equation can be written in differential form as

$$-\alpha_f \hat{\mu}_f \frac{\partial^2 \hat{u}_f}{\partial \hat{z}^2} + \frac{1}{2} C_d \hat{\rho}_f \hat{u}_f^2 \hat{S} = \frac{\Delta \hat{p}}{\hat{L}}, \quad (1)$$

where u_f is the fluid velocity and α_f is the fluid fraction.

The temperature field in a fluid is described by a balance between thermal convection in the streamwise direction, thermal diffusion and convective heat transfer from the fluid to the solid. Thus, the differential form of the energy equation for the fluid is

$$\alpha_f \hat{\rho}_f \hat{c}_f \hat{u}_f \frac{\partial \hat{T}_f}{\partial \hat{x}} = \alpha_f \hat{\lambda}_f \frac{\partial^2 \hat{T}_f}{\partial \hat{z}^2} - \hat{h}\left(\hat{T}_f - \hat{T}_s\right)\hat{S}, \quad (2)$$

where T_f is the fluid temperature and T_s is the solid structure temperature. The heat transfer between the solid and the fluid is modeled as a linear relation between both temperatures, where *h* is a local heat transfer coefficient.

The chip cooler structure in each control volume is only loosely connected in the horizontal directions. As a consequence, only the thermal diffusion in the vertical direction is in balance with heat leaving the structure through the fluid-solid interface, whereas the thermal diffusion in the horizontal directions can be neglected. This simplifies the energy equation for the solid structure to

$$0 = \alpha_s \hat{\lambda}_s \frac{\partial^2 \hat{T}_s}{\partial \hat{z}^2} + \hat{h}\left(\hat{T}_f - \hat{T}_s\right)\hat{S}, \quad (3)$$

where α_s is the solid fraction.

Equations (1-3), written with the phase averaged variables, are dimensional equations for steady-state transport of momentum and heat through homogeneous porous media. Reliable empirical data for the two additional parameters, the local drag coefficient C_d and the local heat transfer coefficient *h*, were found in [7-9].

SIMULATION DOMAIN

The geometry of the simulation domain as well as the boundary conditions for eqs. (1-3) follow the geometry of the experimental test section used in the Morrin-Martinelli-Gier Memorial Heat Transfer Laboratory at University of California, Los Angeles, where experimental data described in [5] were taken.

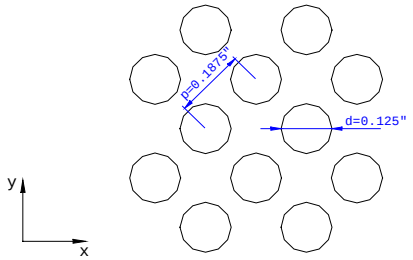

Figure 2: Pin-fins arrangement in the simulated case.

The general arrangement of pin-fins in the simulation domain is given in Fig. 2. The diameter of the pin-fins is d = 0.003175m (0.125''). The pitch-to-diameter ratio in the streamwise direction is p_x/d = 1.06 and in the transverse direction is p_y/d = 2.12. The simulation domain consisted of 34 rows of pin-fins in the streamwise direction and 17 rows of pin-fins in the transverse direction.

Due to the two-dimensionality of the semi-analytical calculation, no-slip boundary conditions for the momentum equation (1) were implemented only on the bottom and top walls, which were parallel with the flow direction:

$$\hat{u}_f(0) = 0, \quad \hat{u}_f\left(\hat{W}\right) = 0. \quad (4)$$

The whole-section pressure drop Δp was imposed as the flow driving force. The absolute values are summarized in Table 1.

For the fluid energy transport equation (2), the simulation domain inflow and the bottom wall were taken as isothermal, whereas the rest of walls were considered as adiabatic:

$$\hat{T}_f(0,\hat{z}) = \hat{T}_{in}, \quad \frac{\partial \hat{T}_f}{\partial \hat{x}}\left(\hat{L},\hat{z}\right) = 0, \quad (5)$$
$$\hat{T}_f(\hat{x},0) = \hat{T}_b, \quad \frac{\partial \hat{T}_f}{\partial \hat{z}}\left(\hat{x},\hat{H}\right) = 0.$$

For the solid structure energy equation (3), the bottom wall was prescribed as isothermal, whereas the top wall was assumed to be adiabatic

$$\hat{T}_s(\hat{x},0) = \hat{T}_b, \quad \frac{\partial \hat{T}_s}{\partial \hat{z}}\left(\hat{x},\hat{H}\right) = 0. \quad (6)$$

The assumption of an isothermal bottom wall, eqs. (5, 6), differs significantly from the experimental set-up [5], where the pin-fins were connected with a conductive base plate. Nevertheless, as the results will show, the present model yields a satisfactory approximation of the measured values.

The absolute temperatures in the different simulation cases are summarized in Table 1.

Table 1: Boundary conditions - preset values.

No.	Δp [Pa]	T_{in} [°C]	T_b [°C]	No.	Δp [Pa]	T_{in} [°C]	T_b [°C]
1	5.0	23.0	103.8	**5**	74.7	23.2	41.8
2	10.0	23.0	74.6	**6**	179.3	23.2	35.7
3	20.0	23.0	58.8	**7**	274.0	23.0	33.6
4	40.0	23.0	48.2	**8**	361.1	22.8	32.3

SOLUTION METHOD

In spite of the availability of more general numerical methods, we tried to find a solution of eqs. (1-6) using a semi-analytical Galerkin approach. To construct the solution method, the transport equations (1-3) were first scaled,

$$-\frac{\alpha_f}{Re_s}\left(\frac{\hat{d}_h^2}{\hat{H}^2}\right)\frac{\partial^2 u_f}{\partial z^2} + \frac{1}{2} C_d \left(\hat{d}_h \hat{S}\right) u_f^2 = \frac{\hat{d}_h}{\hat{L}}, \quad (7)$$

$$\alpha_f \, Pr \, Re_s \left(\frac{\hat{d}_h}{\hat{L}} \right) u_f \, \frac{\partial T_f}{\partial x} = \alpha_f \left(\frac{\hat{d}_h^2}{\hat{H}^2} \right) \frac{\partial^2 T_f}{\partial z^2} - Nu_s \left(\hat{d}_h \hat{S} \right) \left(T_f - T_s \right), \tag{8}$$

$$0 = \alpha_s \left(\frac{\hat{d}_h^2}{\hat{H}^2} \right) \frac{\partial^2 T_s}{\partial z^2} + Nu_s \left(\frac{\hat{\lambda}_f}{\hat{\lambda}_s} \right) \left(\hat{d}_h \hat{S} \right) \left(T_f - T_s \right), \tag{9}$$

and then linearized

$$-M_2 \frac{\partial^2 u_f}{\partial z^2} + K u_f = M_4, \tag{10}$$

$$F_1 u_f \frac{\partial T_f}{\partial x} = F_4 \frac{\partial^2 T_f}{\partial z^2} - F_5 \left(T_f - T_s \right), \tag{11}$$

$$0 = S_1 \frac{\partial^2 T_s}{\partial z^2} + S_2 \left(T_f - T_s \right), \tag{12}$$

where M_2, K, M_4, F_1, F_4, F_5, S_1 and S_2 were taken as constants.

The transport equation scaling transforms the boundary conditions (4-6) into the form

- $u_f(0)=0$, $u_f(1)=0$, (13)
- $T_f(0,z)=1$, $\partial T_f/\partial z(1,z)=0$, $T_f(x,0)=0$, $\partial T_f/\partial z(x,1)=0$,
- $T_s(x,0)=0$, $\partial T_s/\partial z(x,1)=0$.

The complete scaling of the transport equations and boundary conditions can be found in [7] and will not be repeated here.

For the prescribed boundary conditions given by eq. (13), a solution of the momentum transport equation (10) can be found directly in closed form,

$$u_f = C_1 \, exp(\gamma z) + C_2 \, exp(-\gamma z) + \frac{M_4}{K}. \tag{14}$$

The energy transport equations (11, 12) are solved using an eigenfunction expansion. The first step is to derive a single equation for the solid temperature T_s using eqs. (11, 12),

$$D_1(z) \frac{\partial T_s}{\partial x} + D_2 \frac{\partial^4 T_s}{\partial z^4} - D_3 \frac{\partial^2 T_s}{\partial z^2} - D_4(z) \frac{\partial^3 T_s}{\partial x \partial z^2} = 0. \tag{15}$$

With separation of variables, $T_s = XZ$, eq. (15) is transformed to

$$D_1 Z X^I + D_2 Z^{IV} X - D_3 Z^{II} X - D_4 Z^{II} X^I = 0. \tag{16}$$

The variable Z is represented by a finite set of orthogonal functions $Z=A_n Z_n$, where $Z_n = sin(\gamma_n z)$ and $\gamma_n=(2n-1)\pi/2$, that satisfy the boundary conditions given by eq. (13) for the isothermal bottom and the adiabatic top wall.

The expansion into a finite series necessarily introduces an error into the approximation

$$X^I A_n \left\{ D_1 + \gamma_n^2 D_4 \right\} Z_n + X A_n \left\{ \gamma_n^4 D_2 + \gamma_n^2 D_3 \right\} Z_n = error. \tag{17}$$

As the *error* is also orthogonal to the set of basis functions used in the expansion, multiplication by Z_m, m=1,n and further integration from 0 to 1 gives

$$X^I A_n \int_0^1 \left\{ D_1 + \gamma_n^2 D_4 \right\} Z_n Z_m dz + X A_n \int_0^1 \left\{ \gamma_n^4 D_2 + \gamma_n^2 D_3 \right\} Z_n Z_m dz = 0 \tag{18}$$

In matrix notation, the system of n equations (18) can be written

$$X^I A_n I_{nm} + X A_n J_{nm} = 0, \tag{19}$$

where I_{nm} and J_{nm} represent integrals, which were solved analytically. A first order differential equation for X_m is obtained from eq. (19),

$$X_m^I + \beta_m X_m = 0, \tag{20}$$

that has an exponential solution form, $X_m \sim \exp(-\beta_m x)$. Furthermore, inserting the exponential solution form of eq. (20) into eq. (19), an extended eigenvalue problem is derived,

$$\left(J_{nm} - \beta_m I_{nm} \right) A_n = 0, \tag{21}$$

that will yield values for β_m and A_n. Using solutions to eqs. (20, 21), one can construct the solid structure temperature field,

$$T_s = C_i X_i A_{in} Z_n, \tag{22}$$

and , by considering eq. (12), the fluid temperature field is given by

$$T_f = C_i X_i A_{in} \left(1 + \frac{S_1}{S_2} \gamma_n^2 \right) Z_n. \tag{23}$$

The coefficients C_i, which are still unknowns, are found from the fluid temperature boundary conditions: $T_f(0, z)=1$.

Calculations were performed using 45 basis functions. The values were calculated on a numerical mesh with 34x60 grid points.

RESULTS AND DISCUSSION

The calculations were performed for the imposed pressure drops summarized in Table 1. The imposed pressure drops resulted in fluid flows with Reynolds numbers ranging from Re_h = 164 to 1898, where the definition of the Reynolds number is based on a hydraulic diameter d_h of a hypothetical porous media channel,

$$Re_h = \frac{\bar{\hat{u}}}{\hat{\nu}_f} \hat{d}_h = \frac{\bar{\hat{u}}}{\hat{\nu}_f} \left(4 \frac{\alpha_f}{\hat{S}} \right). \tag{24}$$

In all cases the heat transfer from the isothermal bottom was adjusted to 125 W to match the experimental setup [5].

A cross-section of temperature fields for some example calculations are presented in Figs. 3 (fluid) and 4 (solid). The double set of isotherms marks temperature fields obtained with three-dimensional finite volume calculation [6] and with semi-analytical Galerkin approach.

The comparison shows that the values are almost identical at the test section inflow, whereas at the outflow the discrepancy raises up to approximately 5 per cent of whole section temperature rise. The discrepancy comes from differences in boundary conditions used in both calculations as well as from linearization of the momentum equation (10).

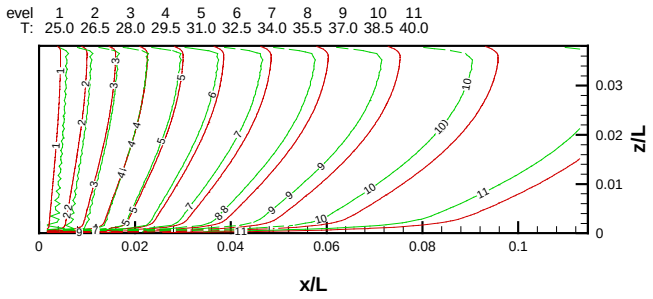

Figure 3: Temperature field in fluid, comparison of results between finite volume method (red) and Galerkin approach (green); Re_h = 782, 125 W of thermal power.

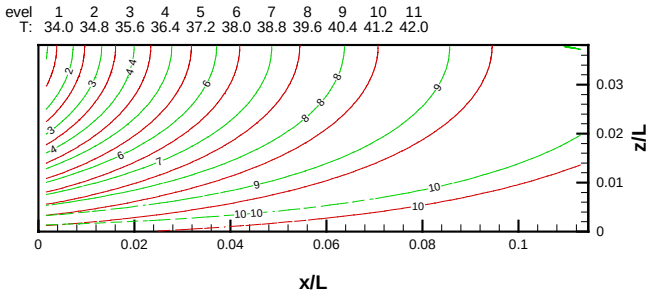

Figure 4: Temperature field in solid, comparison of results between finite volume method (red) and Galerkin approach (green); Re_h = 782, 125 W of thermal power.

The isotherms in Figs. 3 and 4 give detailed insight into the test section temperature distributions. Fig. 3 shows how air is gradually heated from the inlet on the left side to the outlet on the right side. The lower part of the temperature field also shows the intensive heating from the isothermal bottom boundary, which results in gradual horizontal thermal stratification of passing air. With increasing thermal power or/and length of the simulation domain, the horizontal stratification becomes stronger.

Fig. 4 presents the temperature field in the solid structure of the heat sink. It shows that the structure has its highest temperature close to the isothermal bottom and the lowest in the upper left edge, where it is exposed to the low-temperature inflow.

More general comparisons of the whole-section drag coefficient C_d ,

$$\overline{C}_d = \frac{2\Delta\hat{p}}{\hat{\rho}_f (\bar{\hat{u}})^2 \hat{L}\hat{S}} \tag{25}$$

and Nusselt number Nu

$$\overline{Nu} = \frac{\hat{Q}\,\hat{d}_h}{(\hat{T}_b - \hat{T}_{in})\hat{A}_b\hat{\lambda}_f} \tag{26}$$

were also made. The results from the semi-analytical Galerkin calculations were compared with the finite volume method results [6] and with experimental data [5].

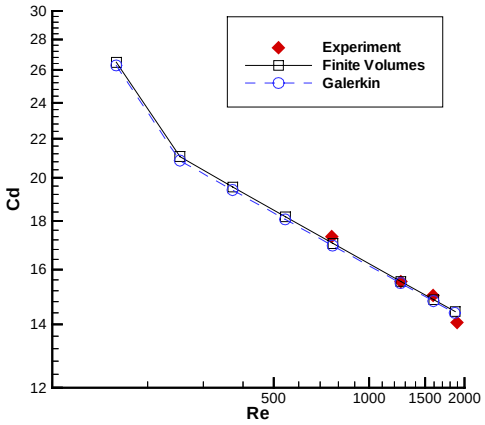

Figure 5: Reynolds number Re_h dependence of drag factor C_d, 125W of thermal power.

The comparison in Fig. 5 shows the whole-section drag coefficient C_d (eq. 25) as a function of the Reynolds number Re_h (eq. 24). It reveals good agreement with the experimental as well as with the finite volume method data.

The comparison of the Nusselt number distributions in Fig. 6 shows good agreement with the finite volume method results, whereas a slight deviation from the experimental data is observed at higher Reynolds numbers. A possible reason for this difference may be that increasing turbulence was not accounted for in either computational model.

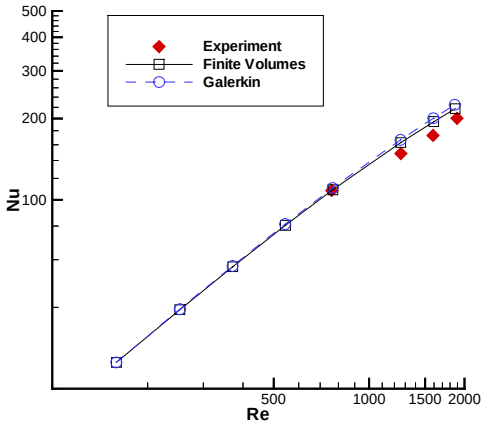

Figure 6: Reynolds number Re_h dependence of Nusselt number Nu, 125W of thermal power.

The design of a heat exchanger involves consideration of both the heat transfer rates and the mechanical pumping power needed to overcome fluid friction and move the fluid through the structure. Thus the main design goal is to maximize the heat transfer rate at minimum pumping power e.g. to increase the heat sink effectiveness Q/W , where

$$\frac{\hat{\dot{Q}}}{\hat{W}} = \frac{c_p \rho (\hat{T}_{out} - \hat{T}_{in})}{\Delta\hat{p}}, \tag{27}$$

at same Reynolds number Re_h.

Fig. 7 shows the effectiveness (eq. 27) as a function of Reynolds number Re_h. The present results are practically identical to the finite volume method results [6] as well as to

the experimental data [5].

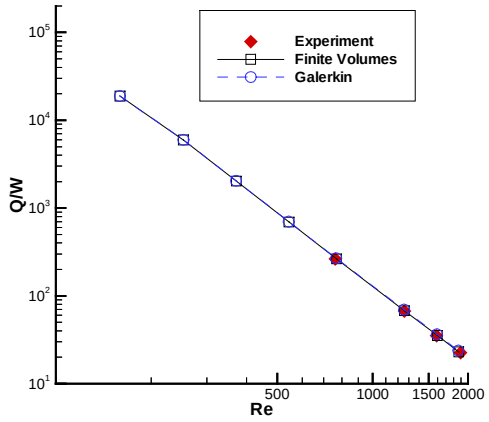

Figure 7: Reynolds number Re_h dependence of heat sink effectiveness Q/W, 125W of thermal power.

As is evident in Fig. 7, the lower Reynolds numbers bring higher effectiveness. Nevertheless, the resulting low heat transfer rates have to be compensated with a larger heat transfer surface and consequently with a larger size of a heat exchanger. In some cases this is not possible due to economics and size limitations. This is why high Reynolds number flow regimes have to be used, although effectiveness is low. Other optimization goals and constraints may better formulate the problem.

CONCLUSIONS

The present paper describes an effort to develop a semi-analytical method for calculation of conjugate heat transfer through a heat sink with a generalized geometry. For that purpose Volume Averaging Technique (VAT) was employed in order to model the heat sink structure as a homogeneous porous media.

Example calculations were made for an aluminum heat sink with staggered pin-fins arrangement cooled with airflow. The geometry of the simulation domain and boundary conditions followed the geometry of the experimental test section used in the Morrin-Martinelli-Gier Memorial Heat Transfer Laboratory at University of California, Los Angeles. The local values of drag and heat transfer coefficients that were needed to close the transport equations were taken from [8-10]. The resulting system of equations was solved with the Galerkin approach using Fourier series expansion in the vertical direction.

To test the calculation procedure, a comparison with finite volume method results [6] and with experimental data [5] was made. The temperature cross-sections in the fluid and the solid show up to a 5 per cent discrepancy when compared to finite volume method results. Furthermore, the calculated values of the whole-section drag coefficient, Nusselt number and heat sink effectiveness show excellent agreement with published data.

The resulting comparisons demonstrate that the Galerkin approach is capable to perform heat exchanger calculations where a thermal conductivity of a solid structure has to be taken into account.

ACKNOWLEDGEMENTS

A. Horvat gratefully acknowledges the financial support received from the Kerze-Cheyovich scholarship and the Ministry of Education, Science and Sport of RS. The efforts of I. Catton were the result of support by DARPA as part of the HERETIC program (DAAD19-99-1-0157).

NOMENCLATURE

A_b	bottom area [m^2]
A_i	interface area [m^2]
A_{in}	eigenvectors [dimensionless]
c_f	fluid specific heat [J/kgK]
C_d	drag coefficient [dimensionless]
C_1	$= -0.5\, M_4\, (1\text{-}exp\ (-\gamma))\,/\,K\ sin\ (\gamma)$ [dimensionless]
C_2	$= 0.5\, M_4 (1\text{-}exp(\gamma))\,/\,K\ sin(\gamma)$ [dimensionless]
d	pin-fin diameter [m]
d_h	hydraulic diameter ($=4\Omega_f/A_i$) [m]
D_1	$= u_f F_1$ [dimensionless]
D_2	$= F_4 S_1 / S_2$ [dimensionless]
D_3	$= F_5 S_1 / S_2 + F_4$ [dimensionless]
D_4	$= u_f F_1 S_1 / S_2$ [dimensionless]
F_1	$= \alpha_f Pr Re_s\, (d_h/L)$ [dimensionless]
F_4	$= \alpha_f\, (d_h^2 / H^2)$ [dimensionless]
F_5	$= Nu_s\, (\, d_h S\,)$ [dimensionless]
h	heat transfer coefficient [W/m^2 K]
H	height of simulation domain [m]
K	$= 1/2 C_d\, (\, d_h S\,)\, u_f$ [dimensionless]
L	length of simulation domain [m]
M_2	$= \alpha_f / Re_s\ (d_h^2 / H^2)$ [dimensionless]
M_4	$= d_h / L$ [dimensionless]
Nu_s	porous Nusselt number ($= h\, d_h / \lambda_f$) [dimensionless]
p	pressure [Pa], pitch [m]
Q	thermal power [W]
Pr	Prandtl number ($=c_f \rho_f \nu_f / \lambda_f$) [dimensionless]
Re_s	porous Reynolds number ($=U\, d_h / \nu_f$) [dimensionless]
S	specific interface surface [1/m]
S_1	$= \alpha_s\, (d_h^2 / H^2)$ [dimensionless]
S_2	$= Nu_s\, (\lambda_f / \lambda_s)\, (\, d_h S\,)$ [dimensionless]
u_f	fluid velocity [m/s], [dimensionless]
T_{in}	inflow temperature [K]
T_f	fluid temperature [K], [dimensionless]
T_s	solid temperature [K] , [dimensionless]
T_b	bottom temperature [K]
U	velocity scale ($= \sqrt{\Delta p / \rho_f}$) [m/s]
x	coordinate in horizontal direct. [m], [dimensionless]
z	coordinate in vertical direct. [m], [dimensionless]

Greek letters

α_f	fluid fraction [dimensionless]
α_s	solid fraction ($1\text{-}\alpha_f$) [dimensionless]
β	eigenvalues [dimensionless]
γ	$\sqrt{K/M_2}$ [dimensionless]
Z	z - dependent part of T [dimensionless]
λ_f	fluid thermal conductivity [W/mK]
λ_s	solid thermal conductivity [W/mK]
μ_f	dynamic viscosity [kg/ ms]
ν_f	kinematic viscosity [m^2/s]
ρ_f	fluid density [kg/m^3]
X	x - dependent part of T [dimensionless]
Ω_f	fluid volume [m^3]

REFERENCES

1. J.E. Hesselgreaves, *Compact Heat Exchangers Selection, Design and Operation*, Pergamon Press, 2001.
2. S. Whitaker, Diffusion and Dispersion in Porous Media, *AIChE Journal*, Vol. 13, No. 3, pp. 420-427, 1967.
3. V. Travkin, I. Catton, A Two Temperature Model for Fluid Flow and Heat Transfer in a Porous Layer, *J. Fluid Engineering*, Vol. 117, pp. 181-188, 1995.
4. V. Travkin, I. Catton, Transport Phenomena in Heterogeneous Media Based on Volume Averaging Theory, *Advans. Heat Trasfer*, Vol. 34, pp. 1-143, 1999.
5. M. Rizzi, M. Canino, K. Hu, S. Jones, V. Travkin, I. Catton, Experimental Investigation of Pin Fin Heat Sink Effectiveness, *Proc. of the 35th National Heat Transfer Conference*, Anaheim, California, 2001.
6. A. Horvat, M. Rizzi, I. Catton, *Advances in Computational Methods In Heat Transfer VIII, Numerical Investigation of Chip Cooling Using Volume Averaging Technique* (*VAT*), Computational Mechanics Publications, Southampton, UK, 2002.
7. A. Horvat, *Calculation of Conjugate Heat Transfer Using Volume Averaging Technique*, M.Sc. Thesis, University of California, Los Angeles, 2002.
8. B.E. Launder, T.H. Massey, The Numerical Prediction of Viscous Flow and Heat Transfer in Tube Bank. *Trans. ASME J. Heat Transfer*, Vol. 100, pp. 565-571, 1978.
9. W.M. Kays, A.L. London, *Compact Heat Exchangers*. 3rd Ed. Krieger Publishing Company, Malabar, Florida, pp. 146-147, 1998.
10. A.A. Žukauskas, R. Ulinskas, Efficiency Parameters for Heat Transfer in Tube Banks. *J. Heat Transfer Engineering*, Vol.5, No.1, pp. 19-25, 1985.